

# Multi-temporal InSAR evidence of ground subsidence induced by groundwater withdrawal: the Montellano aquifer (SW Spain)

Ana Ruiz-Constán<sup>1</sup> · Antonio M. Ruiz-Armenteros<sup>2,3,4</sup> · Francisco Lamas-Fernández<sup>5</sup> · Sergio Martos-Rosillo<sup>1</sup> · J. Manuel Delgado<sup>3,6</sup> · David P. S. Bekaert<sup>7</sup> · Joaquim João Sousa<sup>8</sup> · Antonio J. Gil<sup>2,3,4</sup> · Miguel Caro Cuenca<sup>9</sup> · Ramon F. Hanssen<sup>10</sup> · Jesús Galindo-Zaldívar<sup>11,12</sup> · Carlos Sanz de Galdeano<sup>12</sup>

Received: 25 March 2015 / Accepted: 12 September 2015 / Published online: 25 January 2016  
© Springer-Verlag Berlin Heidelberg 2015

**Abstract** This study uses the InSAR technique to analyse ground subsidence due to intensive exploitation of an aquifer for agricultural and urban purposes in the Montellano town (SW Spain). The detailed deformation maps clearly show that the spatial and temporal extent of subsidence is controlled by piezometric level fluctuations and the thickness of compressible sediments. The total vertical displacement measured with multi-temporal InSAR, between 1992 and 2010, is 33 mm that corresponds with a decrease of 43 m in the groundwater level. This technique allows monitoring the evolution of settlement related to water level fall in an area where subsidence has not yet been reported by population or authorities through infrastructure damages and to discuss the effect of the aquifer recovery. This information is, therefore, valuable for implementing effective groundwater management schemes and land-use planning and to propose new building regulations in the most affected areas.

**Keywords** InSAR · Radar interferometry · Subsidence · Deformation · SW Spain · Aquifer

## Introduction

Natural hazards and their relationship with land-use planning have been the main focus of research together with the development of methodologies to assess them (Mitchel 1998). Among others, ground deformation has been reported as a main task in planning present-day human settlements (Wang et al. 2004). World population increases has compelled to the occupation of less suitable territories. In this context, ground subsidence induced by intensive aquifers exploitation to meet the needs of the rapid evolving industries and urbanization has become particularly relevant (Hu et al. 2004; Perissin and Wang 2011). This phenomenon, the consolidation of the aquifer system

✉ Ana Ruiz-Constán  
a.ruiz@igme.es

<sup>1</sup> Instituto Geológico y Minero de España, Ríos Rosas 23, 28003 Madrid, Spain

<sup>2</sup> Departamento de Ingeniería Cartográfica, Geodésica y Fotogrametría, Universidad de Jaén, Campus Las Lagunillas s/n, 23071 Jaén, Spain

<sup>3</sup> Grupo de Investigación Microgeodesia Jaén, Universidad de Jaén, Campus Las Lagunillas s/n, 23071 Jaén, Spain

<sup>4</sup> Centro de Estudios Avanzados en Ciencias de la Tierra (CEACTierra), Universidad de Jaén, Campus Las Lagunillas s/n, 23071 Jaén, Spain

<sup>5</sup> Departamento de Ingeniería Civil, Universidad de Granada, ETSICCP, Avda. Fuentenueva, s/n, 18071 Granada, Spain

<sup>6</sup> Progressive Systems Srl, Rome, Italy

<sup>7</sup> COMET, School of Earth and Environment, University of Leeds, Leeds, UK

<sup>8</sup> Escola de Ciências e Tecnologia, Universidade de Trás-os-Montes e Alto Douro, Vila Real, Portugal

<sup>9</sup> Department of Radar Technology, TNO, The Hague, The Netherlands

<sup>10</sup> Department of Geoscience and Remote Sensing, Delft University of Technology, Delft, The Netherlands

<sup>11</sup> Departamento de Geodinámica, Universidad de Granada, 18071 Granada, Spain

<sup>12</sup> Instituto Andaluz de Ciencias de la Tierra, CSIC-Universidad de Granada, 18071 Granada, Spain

(aquifers and aquitards), has a huge socio-economic impact as it affects wide areas and many cities along the world—Mexico D.F., Shanghai (China) or Bangkok (Thailand)—(Osmanoglu et al. 2011; Chai et al. 2004; Aobpaet et al. 2013). Precisely evaluating long-term response to pumping and recharge is of great importance to avoid heavy expenses to the local or national administrations due to damages to infrastructures, decrease in water resources or water contamination (Ortiz-Zamora and Ortega-Guerrero 2010).

InSAR data applied to ground displacements, when combined with information about groundwater levels and management practices, have contributed to the hydrogeologic understanding of aquifers (Amelung et al. 1999; Galloway and Hoffmann 2007; Davila-Hernandez et al. 2014). General subsidence due to water withdrawal has been previously described in Spain at the cities of Murcia (Rodríguez Ortiz and Mulas 2002; Tomás et al. 2005) and Granada (Sousa et al. 2007, 2010, 2011; Fernández et al. 2009), at rates of up to 10 mm/year.

The aim of this contribution is to determine the pattern and timing of the aquifer system response to pumping and successive natural recharge in an intensively exploited aquifer in the Montellano area (SW Spain). We focus on the relationship between lithology

and differential settlement through the analysis of the results obtained with the multi-temporal InSAR (MTI-InSAR) technique. The dataset consists of 51 ERS-1/2 SAR and 20 Envisat ASAR scenes acquired from June 1992 to July 2000 and from February 2003 to September 2010, respectively. These results are compared with the current stress history of soils in the area, expressed as the preconsolidation stress and the overconsolidation ratio (OCR) to establish the future behaviour of soils related to the pumping activity.

## Geological and hydrogeological setting

The study area is located in the external zones of the western Betic Cordillera (Fig. 1). Its tectonic structure is characterized by a detached NE–SW to ENE–WSW fold-and-thrust belt (Kirker and Platt 1998). The frontal sector is progressively more deformed toward the west and is disrupted into Mesozoic carbonated blocks—up to several kilometres long—surrounded by a Miocene *mélange* unit mainly consisting of viscous Triassic clays and gypsum (Martín-Algarra and Vera 2004; Pedrera et al. 2012). This structure conditions the reduced extension and complex geometry of the aquifers in this area.

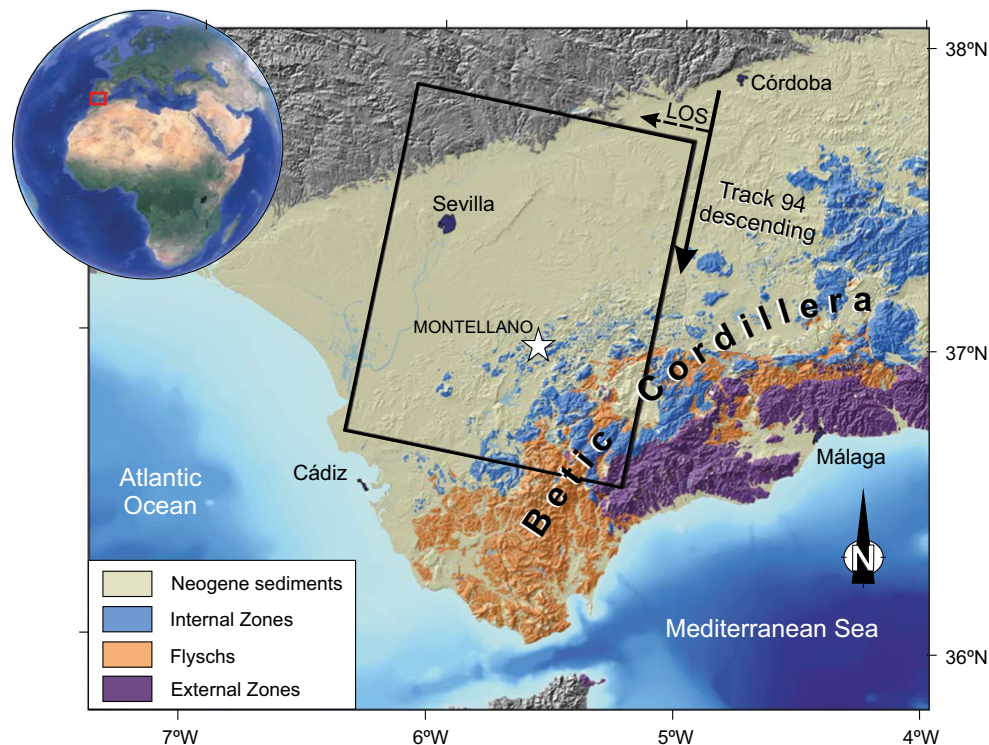


**Fig. 1** Location of the study area in the geological context of the Betic Cordillera. The SAR data coverage used in the study is indicated by a *black rotated box*, indicating with an *arrow* the

descending satellite pass (*track*). The radar is most sensitive to deformation in the radar line-of-sight (LOS), *dashed arrow*. Our study area, Montellano, is indicated by the *star*

The study zone corresponds to Montellano (Seville), a town in SW Spain (Fig. 2). It was developed by occupying the plain in the western side of the San Pablo carbonate range. The aquifer was not exploited up to the 1990s since the use of running river water was more common. However, changes in agricultural practices from non-irrigated to irrigated land favoured intensive groundwater exploitation. The area has a Mediterranean type climate, with an average annual precipitation of 720 mm and an average annual temperature of 18 °C (Durán-Valsero et al. 2003). In this context, a severe drought period from 2004 to 2010 increased the effect on groundwater reserves.

The Montellano aquifer (Fig. 2), with an outcropping surface of 23 km<sup>2</sup>, is divided into two sectors (Durán-Valsero et al. 2003). The eastern or carbonate one is constituted by up to ~600–800 m of Jurassic carbonate rocks (6 km<sup>2</sup>) confined toward the west by an aquitard mélange unit mainly constituted by clays and gypsum (IGME 1988). The western or detritic sector is formed by 17 km<sup>2</sup> of Mio-Pliocene to Quaternary sediments in contact with clays and gypsum at its base. Its stratigraphic sequence starts with Upper Miocene sandy marls and calcarenites (~20 m) and Lower Pliocene yellow sands and calcarenites of up to

60 m thick. Over them, there are ~20 m of Middle Pliocene green clays superposed by ~20 m of Upper Pliocene limestones with gastropods. Finally, at the top of the sequence, there are alluvial and colluvial sand, silts and gravels of Quaternary age.

Recharge of the aquifer is mainly due to the rainfall water infiltration with estimated rates of 25 % for the detritic sediments and 50 % for the carbonate rocks. Transmissivity values are scarce but, in average, are around 10 m<sup>2</sup>/days (Durán-Valsero et al. 2003). The main output of the system is the pumping activity for human consumption and agricultural irrigation. The height and temporal evolution of the groundwater level (Fig. 3), north and south of the main thrust that deforms the carbonate range, reveals different hydrogeological behaviour. In the northern half of the aquifer, the piezometric level remains stable through time (Fig. 4; P4 and P5) and the springs remain active although with low flow rates (around 2 L/s). Extractions are mainly located in the southern half (Fig. 2; P1, P2 and P3) where a high cumulated decrease of the groundwater level could be observed (Fig. 3; 45 m from 1993 to 2010 in P1). In the last years, a water salinity increase has been observed in the wells located in the

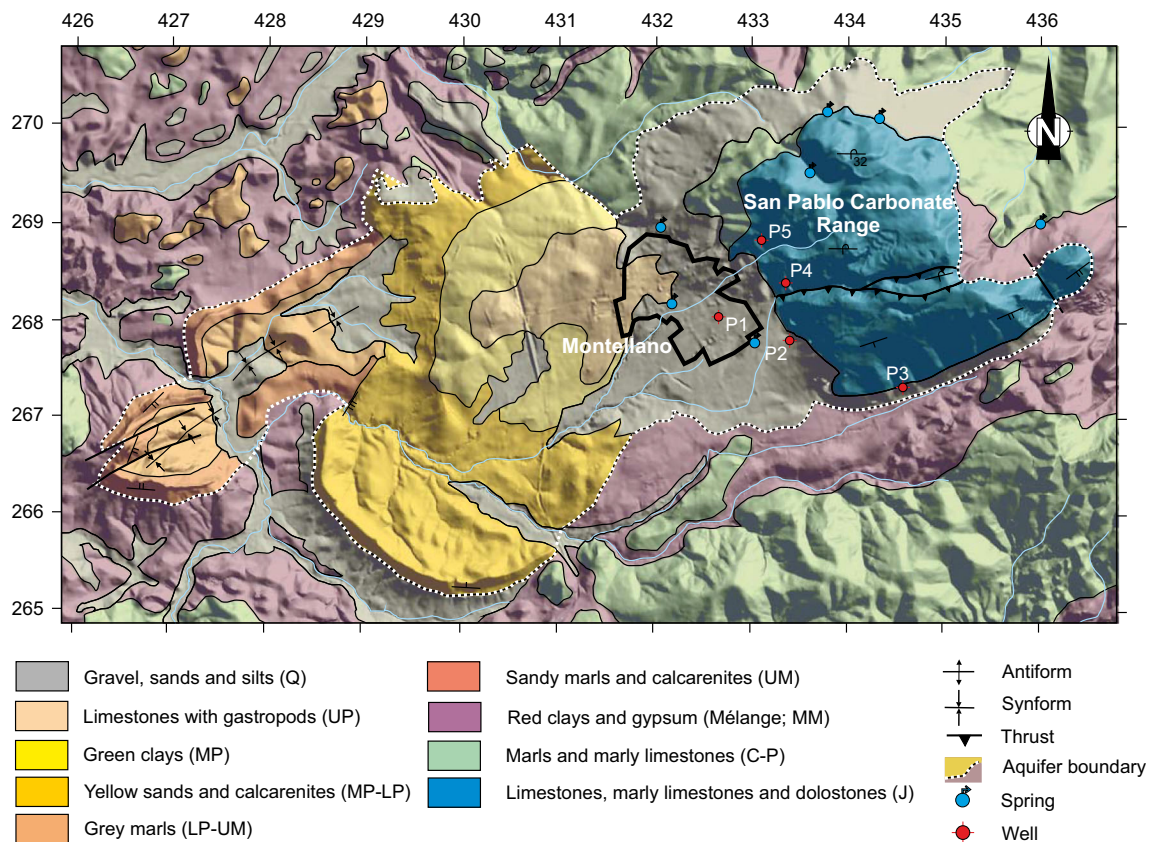


**Fig. 2** Hydrogeological map of the Montellano aquifer; UTM coordinates in km, zone 30S. *Q* quaternary, *UP* upper Pliocene, *MP* middle Pliocene, *LP* lower Pliocene, *UM* upper Miocene, *MM* middle Miocene, *C–P* Paleogene–Cretaceous, *J* Jurassic



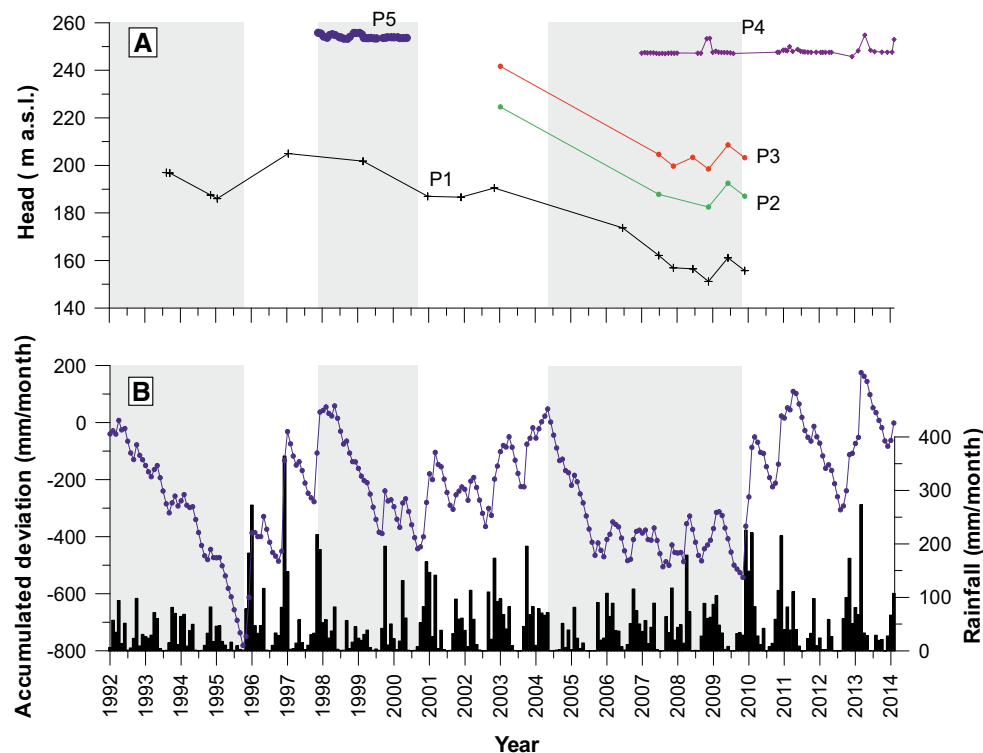


**Fig. 3** **a** Evolution of the piezometric level and **b** rainfall (red bars) together with accumulated deviation of monthly precipitation (blue line), for the period 1992–2013 in the Montellano area. The

piezometer data shown in **a** are sampled at the sounding locations P1–5 shown in Fig. 2. Drought periods correspond to grey-shaded areas

southern sector. This process may be related to the high exploitation rates of the carbonate aquifer that produces a mixture of the bicarbonate waters with the sulphate-enriched waters coming from the clays and gypsum unit.

## Data

### Meteorological and hydrogeological data

Time evolution of the piezometric level (Fig. 3a), together with meteorological data, rainfall and accumulated deviation of monthly precipitation with respect to the average (Fig. 3b), is analysed from 1992 to 2013 to infer inter-connection with the deformation pattern. The data come from the nearest pluviometric station of the Junta de Andalucía network, located in Los Molares, 20 km north-westward of Montellano. The accumulated deviation of monthly precipitation (blue line) gives an estimate of the relative deficit or surplus of precipitation. To calculate it, the average monthly precipitation is obtained for a long-term period (here, 1992–2013) and then this value is successively subtracted to the precipitation value for each month.

Several drought periods could be easily recognized along the trend of the rainfall accumulated deviation: 1992–1995, 1998–2001 and 2004–2009. Concurrently, the piezometric evolution shows a particular hydrological behaviour. First of all, an evident decaying tendency for the piezometric level is observed in the piezometers located at the detritic aquifer (P1, P2 and P3) together with a fast recovery after rainy periods (1996–1998 and 2002–2004). Secondly, a very stable groundwater level is registered in the piezometers located at the carbonate aquifer.

For the first one drought period, the water level decrease was registered at P1 piezometer (13 m). During the other two drought periods, the decrease was 15 and 37 m, respectively, with a mimetic pattern in the P1, P2 and P3 wells. Over the whole period, from 1993 till 2009, the excessive pumping of the aquifer caused an average decrease of 45 m in the groundwater levels as observed at P1 (Fig. 4). For P2–5, piezometric data available are discontinuous because of the change in the water management agencies responsible of water level records (IGME, TRAGSA, CHG), thus we are not able to precisely address the contribution of each extraction well to subsidence.

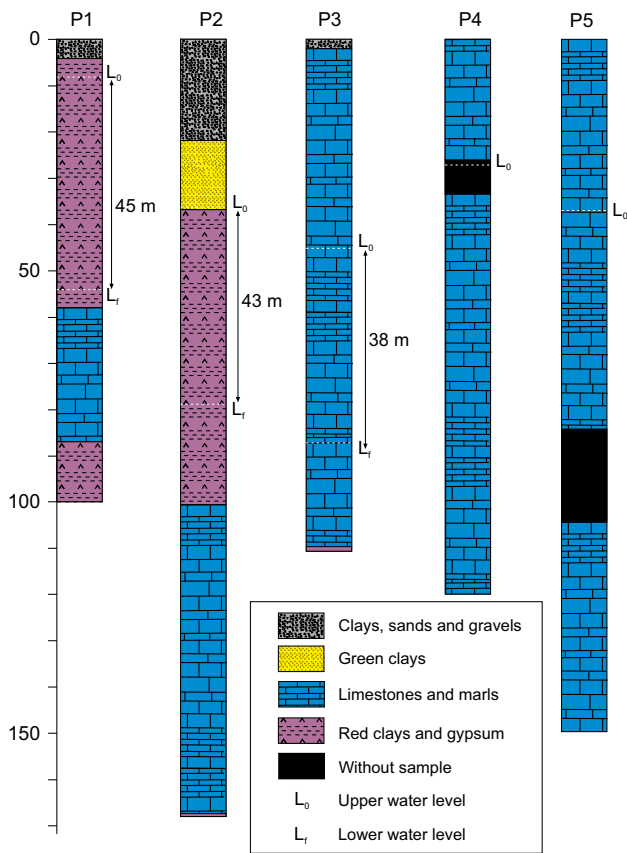


**Fig. 4** Lithological column of the piezometric boreholes, with estimated decrease of water table

**Satellite datasets**

The Montellano area is covered by a total of 51 ERS-1/2 SAR scenes from descending satellite track 94 from June 1992 to July 2000 (Table 1), and by a total of 20 Envisat ASAR scenes from descending satellite track 94 from February 2003 to September 2010 (Table 2). Figure 1 shows the location of this track, which is the same for both satellites, over the study area. Due to ERS-2 on-board gyroscope problems on January 2001, only images until the end of 2000 were selected to avoid high Doppler centroid differences of more than the critical value of 700 Hz.

**Soil samples**

Fifty undisturbed samples of sediments and carbonated rocks from the Montellano aquifer area have been characterized (Table 3). They represent the main lithologies cropping out in the region: Jurassic limestones, red clays from the melange, the Miocene sandy marls and clays and the Quaternary deposits. The preconsolidation stress and the overconsolidation ratio have been obtained (“Geotechnical characterization and tense-deformational

behaviour”) as they are the two main parameters that allow us to determine the tense-deformational information.

**MTI-InSAR**

**Processing methodology**

Differential synthetic aperture radar (SAR) interferometry (DInSAR), first introduced in 1974 for topographic mapping, is a cost-effective measuring geodetic technique used to detect changes on the ground surface with a centimetre-to-millimetre accuracy at a spatial resolution of tens-of-metres over a large area (Gabriel et al. 1989). DInSAR systems are based on extracting the phase difference from two single-look complex (SLC) SAR images relative to the same area by creating an InSAR image (also called an interferogram). The interferometric phase  $\Delta\phi_{int}$ , or difference in the line-of-sight (LOS) path length  $\Delta R$  from the radar antenna to the surface (Fig. 5), in the original interferogram contains the superposition of the following contributions:

$$\Delta\phi_{int} = \Delta\phi_{flat} + \Delta\phi_{topo} + \Delta\phi_{disp} + \Delta\phi_{atm} + \Delta\phi_{noise} \quad (1)$$

where  $\Delta\phi_{flat}$  (also  $\Delta\phi_{orb}$ ) is the phase difference due to differences in the satellite orbits when the two SAR images were acquired (changes of the relative distance satellite-target for flat earth),  $\Delta\phi_{topo}$  is the phase difference due to topography,  $\Delta\phi_{atm}$  is the phase difference due to atmospheric propagation delays,  $\Delta\phi_{disp}$  is the phase difference due to the ground displacement in the slant-range direction, or LOS, between both SAR acquisitions, and  $\Delta\phi_{noise}$  is the systematic and environmental noises. Since the incidence angle of the ERS and Envisat data used in this study is  $\theta \sim 23^\circ$  (ERS-1/2 SAR and Envisat ASAR Image Swath IS2) (Fig. 5), the interferometric phase is more sensitive to vertical displacements.

To estimate ground deformation  $\Delta\phi_{disp}$ , the different phase contributions have to be determined by means of differential processing.  $\Delta\phi_{flat}$  and  $\Delta\phi_{topo}$  depend on the perpendicular baseline and can be calculated accurately using precise satellite orbit data and a digital elevation model (DEM). However, large temporal and satellite separation between both SAR acquisitions (perpendicular baselines), as well as DEM errors, add decorrelation noise due to a change in scattering characteristics of the ground objects over time. On the other hand, atmospheric artefacts  $\Delta\phi_{atm}$ , that is, the atmospheric conditions in both troposphere and ionosphere, can vary considerably between both SAR acquisitions causing phase disturbances. The latter is only significant for dispersive frequencies, like L-band SAR systems, and is not applicable to our study in which C-band data from Envisat and ERS is used. The

**Table 1** ERS-1/2 SAR data for the Montellano area (Track 94 descending, Frame 2859)

	Acq. date	Orbit	Sensor	$B_{\perp}$ (m)	$B_{temp}$ (days)	$f_{dc}$ (Hz)	No.	Acq. date	Orbit	Sensor	$B_{\perp}$ (m)	$B_{temp}$ (days)	$f_{dc}$ (Hz)
1	12/06/1992	4748	ERS-1	460	-1879	415	27	<b>04/08/1997</b>	<b>11,972</b>	<b>ERS-2</b>	<b>0</b>	<b>0</b>	<b>97</b>
2	17/07/1992	5249	ERS-1	-125	-1844	388	28	08/09/1997	12,473	ERS-2	497	35	113
3	21/08/1992	5750	ERS-1	161	-1809	367	29	13/10/1997	12974	ERS-2	430	70	119
4	30/10/1992	6752	ERS-1	898	-1739	378	30	17/11/1997	13,475	ERS-2	289	105	117
5	04/12/1992	7253	ERS-1	132	-1704	411	31	26/01/1998	14,477	ERS-2	-166	175	111
6	08/01/1993	7754	ERS-1	-322	-1669	389	32	02/03/1998	14,978	ERS-2	-700	210	97
7	12/02/1993	8255	ERS-1	437	-1634	364	33	11/05/1998	15,980	ERS-2	729	280	161
8	23/04/1993	9257	ERS-1	834	-1564	401	34	15/06/1998	16,481	ERS-2	966	315	150
9	28/05/1993	9758	ERS-1	-156	-1529	401	35	20/07/1998	16,982	ERS-2	-520	350	143
10	02/07/1993	10,259	ERS-1	-356	-1494	373	36	24/08/1998	17,483	ERS-2	-89	385	151
11	06/08/1993	10,760	ERS-1	450	-1459	378	37	28/09/1998	17,984	ERS-2	813	420	142
12	10/09/1993	11,261	ERS-1	846	-1424	398	38	02/11/1998	18,485	ERS-2	946	455	143
13	19/11/1993	12,263	ERS-1	804	-1354	364	39	07/12/1998	18,986	ERS-2	-367	490	160
14	16/04/1995	19,621	ERS-1	105	-841	384	40	22/03/1999	20,489	ERS-2	134	595	232
15	21/05/1995	20,122	ERS-1	-54	-806	407	41	26/04/1999	20,990	ERS-2	-350	630	184
16	30/07/1995	21,124	ERS-1	448	-736	371	42	13/09/1999	22,994	ERS-2	-704	770	99
17	31/07/1995	1451	ERS-2	411	-735	84	43	18/10/1999	23,495	ERS-2	-256	805	114
18	04/09/1995	1952	ERS-2	-341	-700	79	44	22/11/1999	23,996	ERS-2	-41	840	142
19	08/10/1995	22,126	ERS-1	618	-666	353	45	27/12/1999	24,497	ERS-2	631	875	190
20	26/02/1996	4457	ERS-2	923	-525	116	46	31/01/2000	24,998	ERS-2	112	910	164
21	19/08/1996	6962	ERS-2	-239	-350	98	47	06/03/2000	25,499	ERS-2	-30	945	-53
22	02/12/1996	8465	ERS-2	877	-245	123	48	10/04/2000	26,000	ERS-2	390	980	-208
23	06/01/1997	8966	ERS-2	-56	-210	163	49	15/05/2000	26,501	ERS-2	981	1015	-234
24	17/03/1997	9968	ERS-2	57	-140	153	50	19/06/2000	27,002	ERS-2	-115	1050	-401
25	26/05/1997	10,970	ERS-2	14	-70	119	51	24/07/2000	27,503	ERS-2	-151	1085	-350
26	30/06/1997	11,471	ERS-2	-226	-35	139							

Parameters are relative to the master acquisition, acquired on 04/08/1997. Perpendicular baselines, temporal baselines, and  $f_{dc}$  Doppler centroid are listed with respect to the master acquisition

bibliography on SAR interferometry is extensive. A detailed review of the main principles can be found in Bamler and Hartl (1998), Massonnet and Feigl (1998), Bürgmann et al. (2000), Rosen et al. (2000), and Hanssen (2001).

Time series InSAR techniques address the problem of decorrelation by identifying a small subset of radar targets, called “Persistent Scatterer” (PS) pixels (also referred to as a “Permanent Scatterer”), that exhibit a stable phase characteristic in time, leading to an improved signal-to-noise ratio. PS pixels often correspond to point-wise scatterers or manmade objects on the Earth’s surface (building, metallic objects, exposed rocks, etc.) which dominate background scattering and maintain reflective characteristics along the series of SAR images. Time series InSAR methods include the persistent scatterer interferometry (PSI) methods and small baseline (SB) techniques.

Because PSI and SB approaches are optimized for resolution elements with different scattering characteristics, they are complementary, and techniques that combine both approaches are able to extract the signal with greater coverage than either method alone (Hooper 2008; Ferretti et al. 2011). In our study we use StaMPS-MTI. The Stanford method for persistent scatterers (StaMPS) is a software package that implements a PSI method developed to work even in terrains devoid of manmade structures and/or undergoing non-steady deformation (Hooper et al. 2012, 2013). In addition, StaMPS-MTI (multi-temporal InSAR) is an extended version of StaMPS that also includes an SB method and a combined multi-temporal InSAR method, allowing the identification of scatterers that dominate the scattering from the resolution cell (PS) and slowly decorrelation-filtered phase (SDFP) pixels, that is, pixels whose phase when filtered decorrelates little over short time

**Table 2** Envisat ASAR data for the Montellano area (Track 94 descending, Frame 2859)

No.	Acq. date	Orbit	Sensor	$B_{\perp}$ (m)	$B_{temp}$ (days)	$f_{dc}$ (Hz)
1	24/02/2003	5158	ASAR	-514	-1925	283
2	15/03/2004	10,669	ASAR	687	-1540	233
3	28/06/2004	12,172	ASAR	-627	-1435	230
4	11/10/2004	13,675	ASAR	340	-1330	231
5	20/12/2004	14,677	ASAR	-104	-1260	237
6	04/04/2005	16,180	ASAR	-482	-1155	241
7	09/05/2005	16,681	ASAR	646	-1120	235
8	18/07/2005	17,683	ASAR	719	-1050	237
9	22/08/2005	18,184	ASAR	355	-1015	246
10	31/10/2005	19,186	ASAR	510	-945	259
11	13/02/2006	20,689	ASAR	-402	-840	258
12	05/03/2007	26,200	ASAR	351	-455	267
13	24/03/2008	31,711	ASAR	231	-70	257
<b>14</b>	<b>02/06/2008</b>	<b>32,713</b>	<b>ASAR</b>	<b>0</b>	<b>0</b>	<b>264</b>
15	29/12/2008	35,719	ASAR	-13	210	260
16	18/05/2009	37,723	ASAR	-58	350	261
17	27/07/2009	38,725	ASAR	-85	420	268
18	31/08/2009	39,226	ASAR	248	455	270
19	16/08/2010	44,236	ASAR	-50	805	284
20	20/09/2010	44,737	ASAR	206	840	276

Parameters are relative to the master acquisition, acquired on 02/06/2008. Perpendicular baselines, temporal baselines, and  $f_{dc}$  Doppler centroid are listed with respect to the master acquisition

intervals (Hooper 2008). The PSI technique identifies phase-stable PS pixels using primarily correlation of their phase in space, not requiring any approximate model of displacements. The SB method uses amplitude dispersion values and then identifies the SDFP pixels performing phase analysis in space and time. Finally, both selections (PS + SDFP) are combined and a 3D phase unwrapping algorithm is applied to isolate the deformation signal, based on these pixels. The inner workings of this software package are described in more detail in Hooper (2008, 2010, 2006) Hooper et al. (2004, 2007), and Sousa et al. (2010, 2011).

A DEM with 25 m resolution provided by the Instituto Geográfico Nacional de España was used to remove the contribution of the topographic phase to the interferometric phase. Using highly precise orbit data for ERS-1/2 and Envisat satellites calculated by TU Delft (Scharroo and Visser 1998) and ESA, the reference phase was computed and subtracted from the interferometric phase.

**MTI-InSAR results**

We applied the StaMPS-MTI method, combining PS and SB approaches, over the Montellano area. For the ERS dataset, we constructed 50 interferograms using the PS

approach, and 182 interferograms using the SB approach (Fig. 6). We used the scene of 4 August 1997 as master date in our network. For the Envisat ASAR dataset, we constructed 19 interferograms based on the PS approach, and 45 interferograms using the SB approach (Fig. 6). There, we used the scene of 2 June 2008 as master date.

For the SB approach, Figs. 1 and 2 of the Appendix show the residuals between the unwrapped phase of the SB interferograms and the estimated SB interferograms when redundancy was removed by inverting to a single master network first. No spatially correlated residuals are identified indicating the absence of unwrapping errors. A sophisticated tropospheric correction like in Bekaert et al. (2015) is not being needed as delay variation over the city is expected to be small.

Figures 7 and 8 show the unwrapped phase in millimetres for each stack of scenes referred to the first interferogram, respectively, for ERS 1/2 and Envisat. Throughout our study, we assumed our InSAR reference area to be centred in the old part of the village. This area showed a stable behaviour in previous processing crops where a different reference area outside the village was chosen. For ERS-1/2 (Fig. 7), it can be seen that the southern part of the city is subjected to a subsidence with respect to the northern part in the period November 1993 to

**Table 3** Geotechnical parameters of the sediments in the study area

Lithology	$\gamma_d$	$e$	$\varphi'$	$\varphi'_r$	$c'$	$c'_r$	$K$	cv	$E_{oed}$	$\sigma'_p$	$\sigma'_o$	OCR	$W_{nat}$	$W_{op}$	$T_{max}$	% < 0.08 mm	A
Clays, sands and gravels	18.19	0.40	25.2	12	29	2	1.96E-05	4.30E-04	108.3	106	126	0.841	14.2	14.98	17.2	61.1	0.54
Green clays	16.7	0.84	20	10.9	35	2	6.30E-08	5.30E-04	35	115	97	1.186	18.3	19.22	6.3	95.3	0.6
Grey marls	16.2	0.50	15.5	12	46	2	8.10E-08	8.70E-04	32	105	157	0.669	12.5	22.21	2	98.8	0.73
Sandy marls	17.08	0.84	24	12	20	4	1.60E-08	3.10E-04	63	104	128	0.813	15.2	18.3	10.1	90.76	0.59
Limestones	21.5		35		1		3.49E-02		427				5.3		30	6.2	
Red clays	18.5	0.48	26	11	21	5	1.50E-07	4.44E-04	41	139	142	0.979	14.48	14.4	17.1	82.32	0.57

$\gamma_d$  specific dry weight (KN/m<sup>3</sup>),  $e$  void index;  $\varphi'$  effective angle of internal friction (deg),  $\varphi'_r$  residual effective angle of internal friction (deg),  $c'$  effective cohesion (KPa),  $c'_r$  residual effective cohesion (KPa),  $K$  permeability constant (cm/s),  $cv$  (cm<sup>2</sup>/s),  $E_{oed}$  elastic deformation modulus(MPa),  $\sigma'_p$  preconsolidation stress (KPa),  $\sigma'_o$  vertical effective strength (KPa),  $OCR$  overconsolidation ratio,  $W_{nat}$  natural humidity (%),  $W_{op}$  optimum humidity (%),  $T_{max}$  maximum particle size (mm), % < 0.08 mm: amount of particles greater than 0.08 mm, A activity

April 1995. A similar pattern of subsidence is also presented in the Envisat data (Fig. 8) in the period November 2005 to May 2009. Figure 9a, b shows the mean SAR amplitude images of the analysed area, computed by averaging all the available SAR images for ERS-1/2 and Envisat dataset, respectively. Figure 9c, d shows the geocoded radar line-of-sight (LOS) velocity, assuming a linear deformation rate, superimposed over a Google Earth image. Note that these four images have different geometries: Figs. 9a and b are in the original radar image space while Figs. 9c and d are geocoded images. The velocity plots are relative to a circular reference area (radius of 50 m) centred in the old part of the village of Montellano, presented by the star.

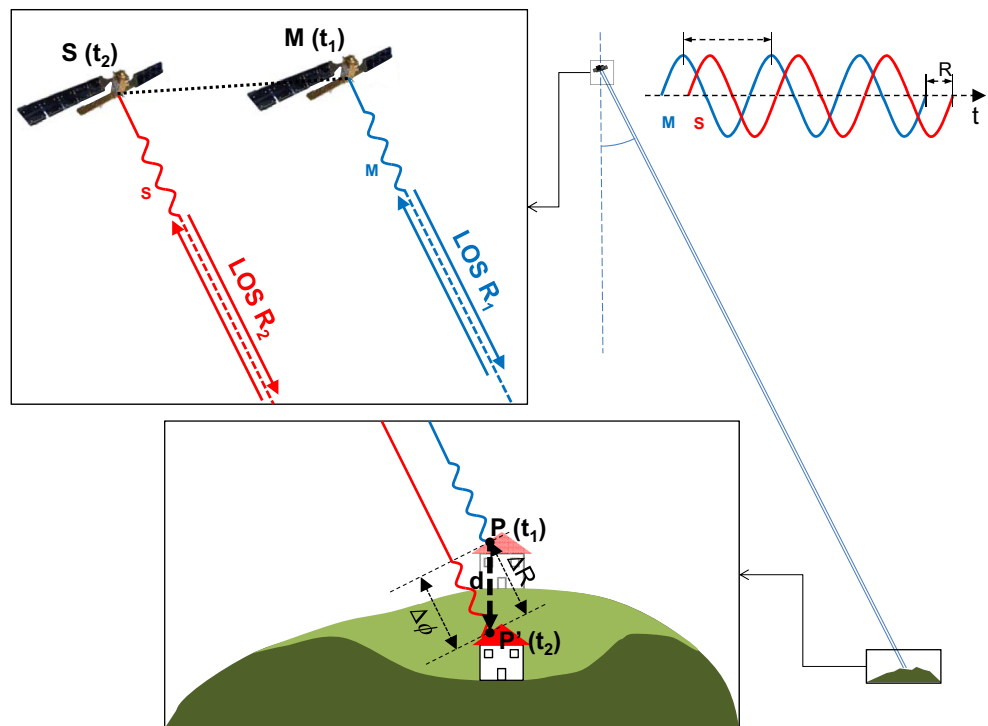
Finally, Fig. 10 shows the displacement time series for the area of larger subsidence in the village, using the PS points within a radius of 50 m represented as P, and the displacement time series for the well P1 (see Fig. 2 for location). No PS points were identified in the surroundings of P2–P5 wells due to temporal decorrelation for forested areas with C-Band. Along the period comprised between 1992 and 2000, we could observe an initial subsidence trend, ending in September 1995, with a total displacement of 11 mm. Later, there is a recovery of 10 mm up to May 1998. The final part of the ERS-1/2 observations is also characterized by subsidence (9 mm) but with a gentler slope. The total displacement recorded for the whole period is of 10 mm, at a rate of 1.5 mm/year. On the other hand, the second period (2004–2009) starts with a very gentle trend of subsidence that sharply changes from the beginning of 2006 up to May 2009. Only after this date we observe a recovery of 6 mm. The total subsidence for the period is 23 mm, at a rate of 4 mm/year.

### Geotechnical characterization and tense-deformational behaviour

Preconsolidation stress ( $\sigma'_p$ ) is the maximum effective stress that a soil has suffered throughout its history. From a geotechnical point of view, it is relevant because it differentiates elastic and reversible deformation from inelastic and partially irreversible deformation revealing the starting point of high compressibility. It also allows us to predict long-term consolidation and differential settlements (Jamiolkowski et al. 1985). The preconsolidation stress for 50 undisturbed samples of sediments and carbonates from the Montellano aquifer area has been studied using the uniaxial consolidation swelling test in accordance with the appropriate international standard ASTM D 4546. We have applied the Casagrande (1936) graphical method, while using the analytical procedure of Sridharan et al. (1991). In addition, to avoid subjective interpretations of the



**Fig. 5** DInSAR basic concept. At  $t_1$ , a point P is sensed. At  $t_2$ , the surface has deformed and point P moves to P'



maximum curvature point (more important when more ductile is the material), we have applied the methodology described by Gregory et al. (2006). Triaxial water permeability test, due to aquitard character of most of the samples, was performed as defined by ASTM D 5084, except for the limestones. In the rest of the tests performed we have followed the procedures proposed by UNE-AENOR.

The results of this test for the red clays and gypsum unit (Middle Miocene) are plotted on a logarithm of the normal effective stress ( $\text{kg}/\text{cm}^2$ ) against void ratio (%), as shown in Fig. 11. These rocks are the ones that widely constitute the lithological column in the subsiding area (P1 and P2; Fig. 4) and those that provide higher consolidation values. The graph shows, for each sample, two different lines. The upper one is characterized by low deformations that are recoverable if unloading occurs. The lower one occurs for higher stresses than the former and it is characterized by its linearity and for the strains being irrecoverable. The point that separates the two lines is the preconsolidation stress. The values obtained are very uniform for all kind of rocks studied (Table 3) and range between 104 and 139 kPa.

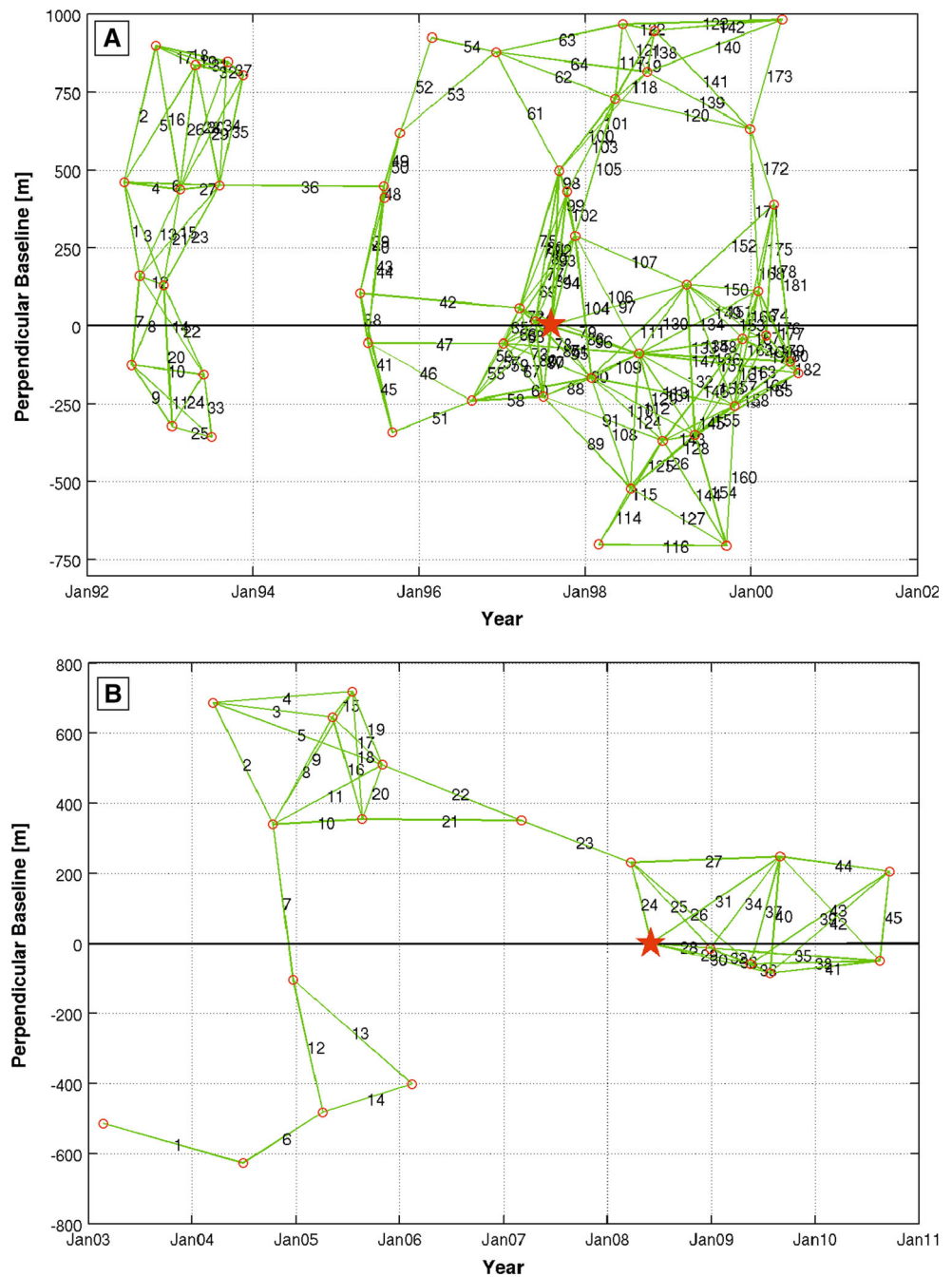
The overconsolidation ratio (OCR) is another useful parameter to complement the tense-deformational information of a soil. This value is the ratio of preconsolidation stress to current natural overburden stress and indicates whether the soil is overconsolidated ( $\text{OCR} > 1$ ), normally consolidated ( $\text{OCR} = 1$ ) or underconsolidated ( $\text{OCR} < 1$ ). A soil is said to be overconsolidated when it has been exposed to vertical effective stresses higher than the ones

acting at present. In this study, we performed consolidated and undrained (CU) triaxial tests in accordance with the appropriate international standard ASTM D 4767. The results show OCR ratio values varying from 0.89 to 1.19, with an average value of 0.90. Accordingly, soils seem to be normally consolidated to slightly underconsolidated close to the surface (unless the green clays samples that provide overconsolidated values). Taking into account the lithology distribution in the surroundings of the P1 well (where the maximum vertical displacement is observed) a subsidence of up to 30 cm is expected, one order of magnitude higher than the vertical displacement estimated with InSAR for the same location. However, it is important to note that this maximum expected subsidence should be higher than the real subsidence as it is evaluated considering surface conditions and for a total compression of the sediments.

**Discussion**

Decrease in pore-water pressure leads to compression of the granular structure of the aquifers (coarse grain deposits) and/or aquitards (silt and clay), and indeed to consolidation of these compressible sediments (Leake 1990; Galloway et al. 1998). In the Montellano aquifer, the decline in pore-water pressure related to groundwater pumping likely controls the land subsidence revealed by the INSAR data in the period 1992–2010. Unfortunately no ASAR data have

**Fig. 6** Temporal vs. spatial baseline distribution for our interferometric ERS-1/2 (a) and ASAR (b) SAR data used in this study (red circles). The master image used in the PSI processing is indicated by the red star. The small baseline interferograms used in the SB processing are represented by the continuous green lines



been acquired after 2010, due to the unexpected loss of contact with Envisat. Associated with this decrease, there was an increase in effective stresses in the subsoil, causing consolidation of the clayey sediments. Analysis of these results has allowed the identification of two main sectors with different ground surface behaviour. The southern sector, placed on recent, deformable quaternary colluvial sediments deposited over Triassic clays and the northern one, over colluvial cemented sediments overlying Middle Pliocene and Jurassic limestones.

The settlement map retrieved from multi-temporal InSAR, combining ERS and Envisat, shows evolution of ground subsidence in the Montellano area. Figure 12 shows the temporal comparison between the vertical displacement observed, the accumulated deviation of monthly precipitation and the evolution of the groundwater level in the piezometer P1, closer to the subsiding area, where a well trend correlation can be distinguished. A maximum of 33 mm of land subsidence for the whole period studied is observed at this sector. Three important subsiding periods

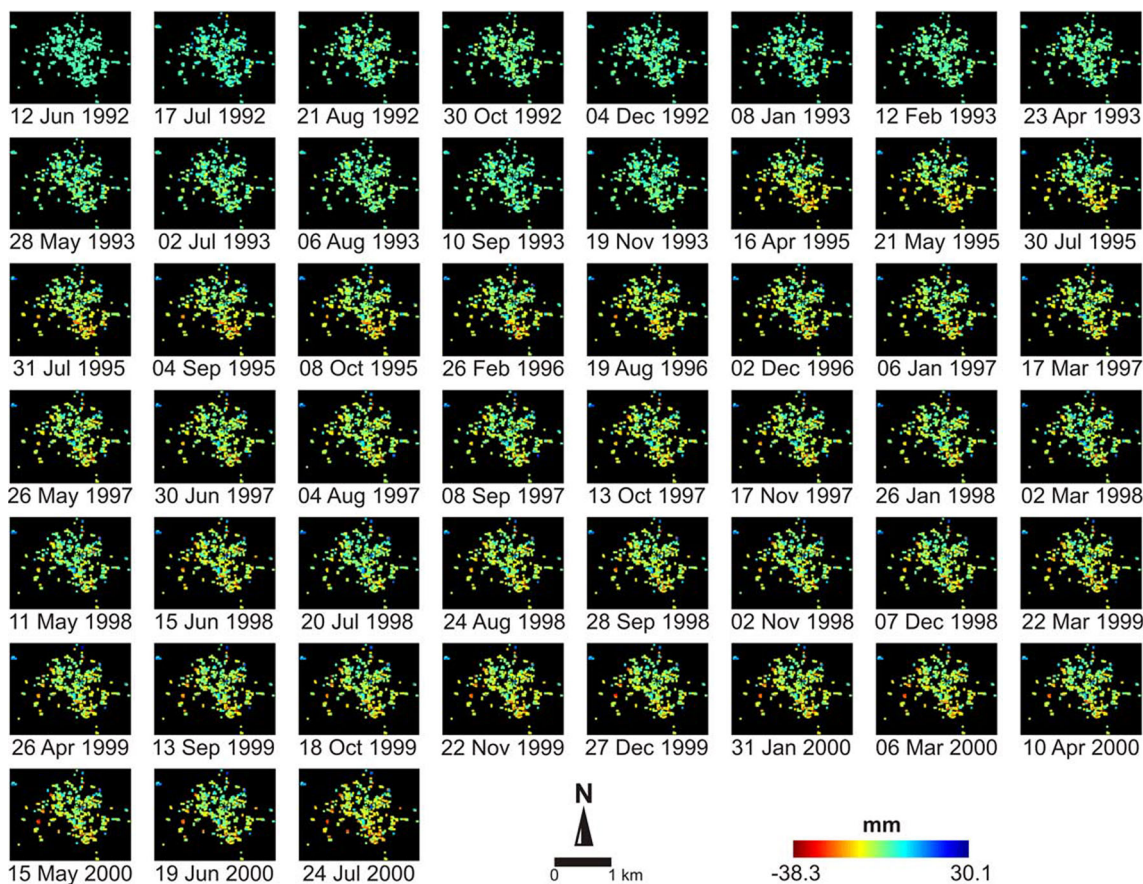


**Fig. 7** Unwrapped phase for the MTI processing (PS + SB) for the ERS-1/2 stack referred to the first data. All the single master interferograms are ordered by dates from *left to right* and *up to bottom*. The unwrapped phase is represented in millimetres

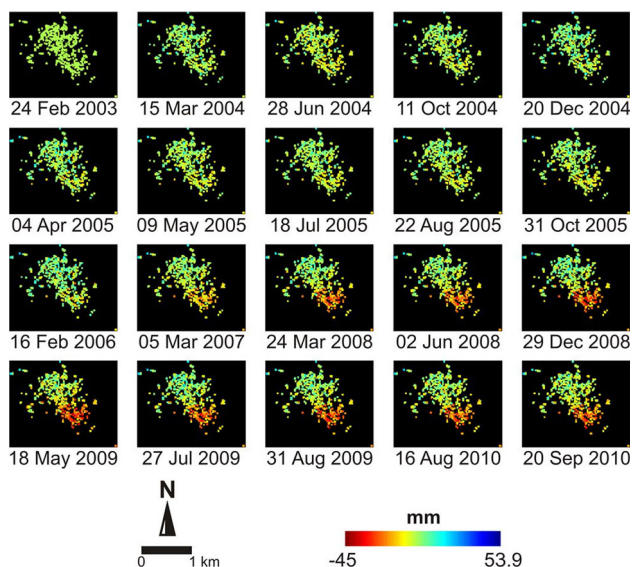


**Fig. 8** Unwrapped phase for the MTI processing (PS + SB) for the ASAR stack referred to the first data. All the single master interferograms are ordered by dates from *left to right* and *up to bottom*. The unwrapped phase is represented in millimetres

could be distinguished, 1992–1995, 1998–2001 and 2004–2009, in tight relationship with the meteorological data and, consequently, with an excessive pumping activity. These fluctuations has been observed in the wells located over the detritic aquifer meanwhile wells located directly over the carbonates show very stable levels in the whole time series. Along the period comprised between 1992 and 2000, the total displacement recorded was of 10 mm, at a rate of 1.5 mm/year. In the period 2001–2002, the piezometric level globally remains stable. Afterwards, the 2004–2010 drought caused a generalized lowering of the piezometric level of 37 m. From 2003 to 2009, the southern area was gradually affected by average settlements that exceeded 23 mm, with typical settlement velocities of about 4 mm/year. This was the most important subsiding period.

Although deformation in an aquifer system is generally elastic and recoverable (Poland 1961), aquitard sediments respond both elastically and inelastically depending upon whether the maximum preconsolidation stresses are exceeded when the piezometric level decreases (Xue et al.



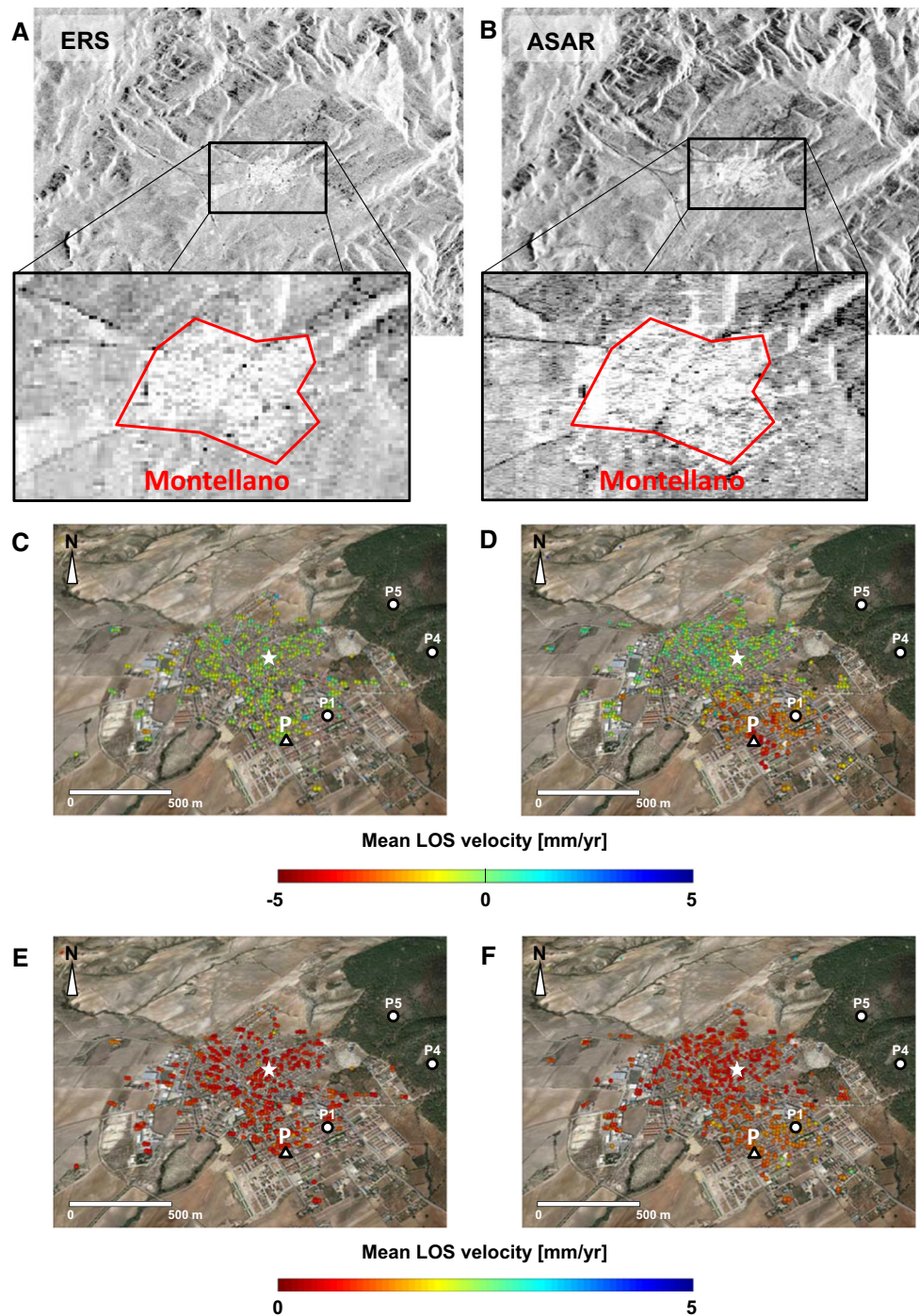


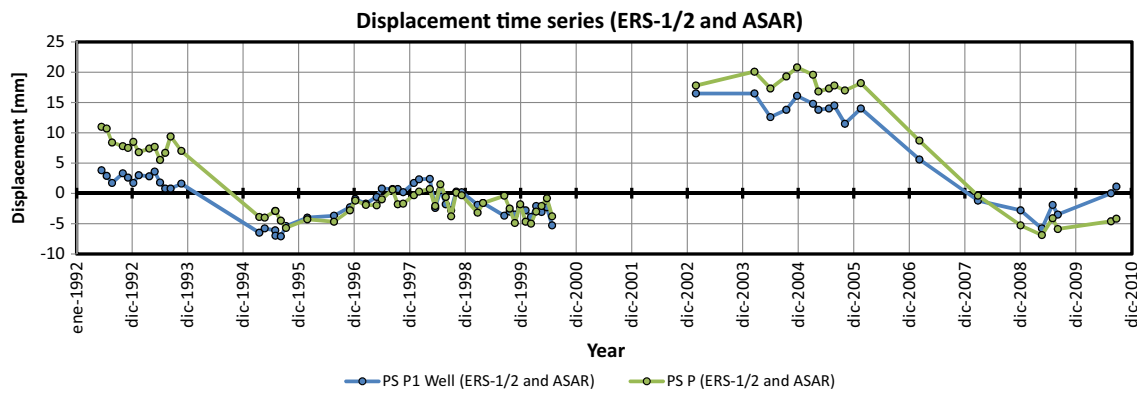
**Fig. 9** **a, b** Mean SAR amplitude images of the study area for ERS-1/2 and ASAR stacks zooming in the village of Montellano. **c, d** Geocoded radar line-of-sight velocity, assuming a linear deformation rate, superimposed over a Google Earth image for ERS-1/2 and ASAR datasets. The *white star* indicates the reference area for phase unwrapping and the *white dots* some wells in the area. The *white*

*triangle* designates the position of an area (*P*) of radius 50 m which exhibits the maximum deformation and which temporal time series is shown in Fig. 10. **e, f** Linear deformation standard deviation for ERS-1/2 and ASAR stacks. ERS-1/2 SAR scenes span the period from June 1992 to July 2000, and Envisat ASAR scenes from February 2003 to September 2010

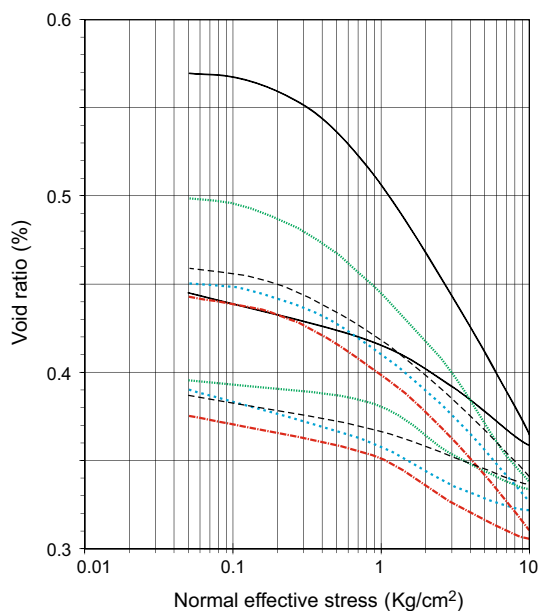
2005). They then undergo a slow, accumulative and irreversible rearrangement of their pore structures. With long-term water-level decline, the aquitards will continue to

exhibit delayed drainage and residual compaction even though groundwater levels in the aquifers may have recovered (Helm 1984; Bell et al. 2008). Such delayed





**Fig. 10** Displacement time series resolved by ERS-1/2 and ASAR descending observations for PS P (the area that exhibits the maximum deformation) and the P1 well. The deformation history is in the LOS direction (see Figs. 2 and 9 for location)



**Fig. 11** Graphical estimation of preconsolidation stress of the red clays

compression is not so evident in the pattern of residual subsidence found in the Montellano aquifer. In 1995, rainfall recharge produced the arising of the groundwater level and this effect was observed, with a small time lag, at the deformation time series.

In many of the affected areas, subsidence has been finally reported after the observation of some local problems as underground utility lines cracking, seawater intrusion or settlements of buildings and civil infrastructures (Tomás et al. 2010; Jiang et al. 2011). Anticipation to this problem will avoid the spending of great amounts of

money, as direct and indirect economic costs, in addressing them. Indeed, much of the subsidence occurring in aquifers subjected to high pumping activity is irrecoverable, resulting in a loss of aquifer storage. This is why the multi-temporal InSAR technique could act as an alarm to draw attention to the excessive withdrawal of groundwater (Chai et al. 2004; Shi and Bao 1984) in areas filled with compressible deposits and thus prone to land subsidence and where these effects are not so evident yet, as in the Montellano area. However, the applicability of this methodology is subject to the spatio-temporal distribution of the piezometric data and the location of geological columnar sections. This information is frequently provided by the national Geological Surveys (as the Instituto Geológico y Minero of Spain in <http://info.igme.es/catalogo/?tab=2>) but its availability differs from one country to another.

Estimation of the spatio-temporal distribution of the settlement is crucial to locate the most damaged areas, to predict their evolution and to establish counter measures to eliminate, or at least mitigate, the causes (Bell et al. 2008; Chaussard et al. 2014). In the Montellano sector, subsidence rates are likely representative of the amount of water extracted and the thickness of the compressible deposits. The southern half of the village is affected by subsidence in the range of 33 mm. The first human settlements were located over the stable Middle Pliocene limestones, in the north part of the present-day village. However, expansion since the 1980s has extended the building area towards the South over uncemented colluvial sediments that overlie Triassic clays, causing consolidation of the clayey sediment layers. Characterization of the subsidence distribution will help to reshape the future urban development plans and better define the urban expansion and land uses.

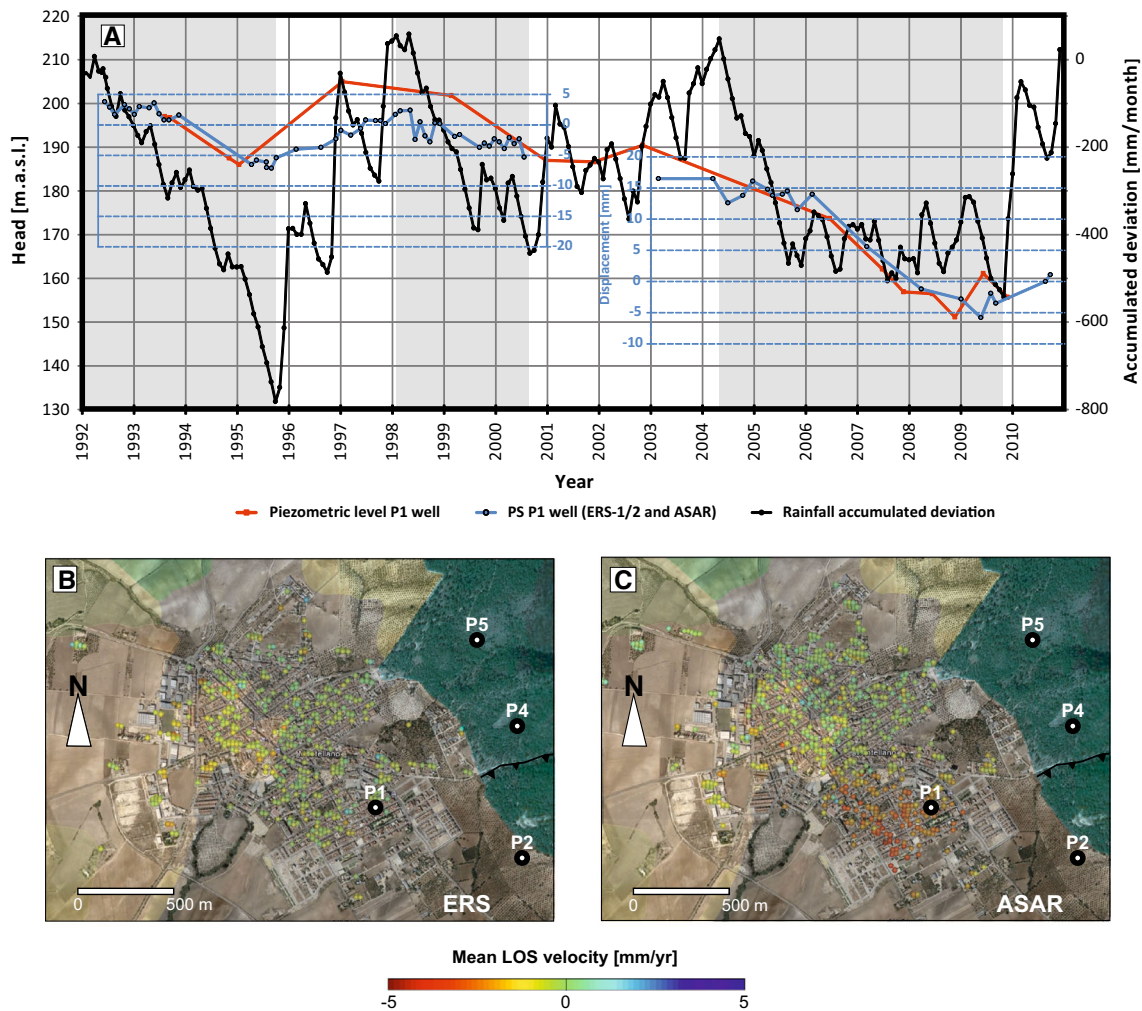


**Fig. 12** a Time evolution of the piezometric level in the P1 well (red line) together with the displacement time series from radar interferometry (blue line) and the rainfall accumulated deviation (black line) for the period 1992–2011. The drought periods are shaded in the plot.

b, c Geocoded radar line-of-sight velocity, assuming a linear deformation rate, superimposed over a Google Earth image for ERS-1/2 and ASAR datasets, respectively; The main geological lithologies are superimposed

## Conclusions

We applied a multi-temporal InSAR technique to analyse ground subsidence due to intensive exploitation of an aquifer for agricultural and urban purposes during the 1992–2010 period in the town of Montellano (SW Spain). We demonstrate that this technique allows monitoring the evolution of settlement related to water level fall in an area where subsidence has not yet been reported by population or authorities through infrastructure damages. In time, we found a correlation between the piezometric level changes and subsidence as observed from InSAR. In addition, interrelation among subsidence and shallow rock distribution has been demonstrated showing that deformations are higher where Triassic clays are thicker in respect to areas where Middle Pliocene or Jurassic limestones crop out. Our study provides valuable information that can be used to

implement effective groundwater management schemes, land-use planning, and to propose new building regulations in the most affected areas. The obtained results provide very useful spatial and temporal data about the incidence of intensive pumping at a low cost.

**Acknowledgments** SAR data are provided by the European Space Agency (ESA) in the scope of 9386 CAT-1 project. This research was supported by PRX 12/00297, ESP2006-28463-E, Consolider-Ingenio 2010 Programme (Topo-Iberia project) CSD2006-0041 (Consolider), AYA2010-15501 projects from Ministerio de Ciencia e Innovación (Spain). In addition, it was supported by the RNM-282 and RNM148 research groups and the P09-RNM-5388 project from the Junta de Andalucía (Spain). The first author has been also funded by a Juan de la Cierva grant (JCI-2011-09178) from Ministerio de Ciencia e Innovación. Interferometric data were processed using the public domain SAR processor DORIS and StaMPS/MTI. The DEM is freely provided by © Instituto Geográfico Nacional de España. The satellite orbits used are from Delft University of Technology and ESA.

## References

- Amelung F, Galloway DL, Bell JW, Zebker H, Laczniak RJ (1999) Sensing the ups and downs of Las Vegas: InSAR reveals structural control of land subsidence and aquifer-system deformation. *Geology* 27(6):483–486
- Aobpaet A, Caro Cuenca M, Hooper A, Trisirisatayawong I (2013) InSAR time-series analysis of land subsidence in Bangkok, Thailand. *Int J Remote Sens* 34(8):2969–2982
- Bamler R, Hartl P (1998) Synthetic aperture radar interferometry. *Inverse Probl* 14:R1–R54. doi:10.1088/0266-5611/14/4/001
- Bekaert DPS, Hooper A, Wright TJ (2015) A spatially-variable power-law tropospheric correction technique for InSAR data. *J Geophys Res Sol Ea*. doi:10.1002/2014JB011558
- Bell JW, Amelung F, Ferretti A, Bianchi M, Novali F (2008) Permanent scatterer InSAR reveals seasonal and long-term aquifer-system response to groundwater pumping and artificial recharge. *Water Resour Res* 44:W02407. doi:10.1029/2007WR006152
- Bürgmann R, Rose PA, Fielding EJ (2000) Synthetic aperture radar interferometry to measure Earth's surface topography and its deformation. *Annu Rev Earth Planet Sci* 28:169–209
- Casagrande A (1936) The determination of pre-consolidation load and its practical significance. *Proceedings of the first international conference on soil mechanics and foundation engineering*, vol 3. Cambridge, England, pp 60–64
- Chai JC, Shen SL, Zhu HH, Zhang XL (2004) Land subsidence due to groundwater drawdown in Shanghai. *Géotechnique* 54(2):143–147
- Chaussard E, Wdowski S, Cabral E, Amelung F (2014) Land Subsidence in central Mexico detected by ALOS InSAR time-series. *Remote Sens Environ* 104:94–106. doi:10.1016/j.rse.2013.08.038
- Davila-Hernandez N, Madrigal D, Expósito JL, Antonio X (2014) Multi-temporal analysis of land subsidence in Toluca valley (Mexico) through a combination of persistent interferometry (PSI) and historical piezometric data. *Adv Remote Sens* 3:49–60. doi:10.4236/ars.2014.32005
- Durán-Valsero JJ, López-Geta JA, Martín-Machuca M, Maestre Acosta A, Pérez Martín P, Mora Fernández P (2003) Atlas hidrogeológico de la provincia de Sevilla. IGME-Diputación Provincial de Sevilla, p 208
- Fernández P, Irigaray C, Jiménez J, Hamdouni R, Crosetto M, Monserrat O, Chacón J (2009) First delimitation of areas affected by ground deformations in the Guadalfeo river valley and Granada metropolitan area (Spain) using the DInSAR technique. *Eng Geol* 105:84–101
- Ferretti A, Fumagalli A, Novali F, Prati C, Rocca F, Rucci A (2011) A new algorithm for processing interferometric data-stacks: SqueeSAR. *IEEE Trans Geosci Remote Sens* 49:3460–3470
- Gabriel AK, Goldstein RM, Zebker HA (1989) Mapping small elevation changes over large areas: differential radar interferometry. *J Geophys Res* 94:9183–9191
- Galloway DL, Hoffmann J (2007) The application of satellite differential SAR interferometry-derived ground displacements in hydrogeology. *Hydrogeol J* 15(1):133–154. doi:10.1007/s10040-006-0121-5
- Galloway DL, Hudnut KW, Ingebritsen SE, Philips SP, Peltzer G, Rogez F, Rosen PA (1998) Detection of aquifer system compaction and land subsidence using interferometric synthetic aperture radar, Antelope valley, Mojave desert, California. *Water Resour Res* 34(10):2573–2585
- Gregory AS, Whaley WR, Watts CW, Bird NRA, Hallet PD, Whitmore AP (2006) Calculation of the compression index and precompression stress from soil compression test data. *Soil Tillage Res* 89:45–57
- Hanssen RF (2001) Radar interferometry: data interpretation and error analysis. Kluwer Academic Publishers, Dordrecht 328 pp
- Helm DC (1984) Field-based computational techniques for predicting subsidence due to fluid withdrawal. In: Holzer TL (ed) *Man-induced land subsidence: reviews in engineering geology* 6: 1–22
- Hooper AJ (2006) Persistent scatterer radar interferometry for crustal deformation studies and modelling of volcanic deformation. Ph.D. thesis, Stanford University
- Hooper A (2008) A multi-temporal InSAR method incorporating both persistent scatterer and small baseline approaches. *Geophys Res Lett* 35:L16302. doi:10.1029/2008GL034654
- Hooper A (2010) A statistical-cost approach to unwrapping the phase of InSAR time series. European Space Agency ESA SP-677 (Special publication)
- Hooper A, Zebker H, Segall P, Kampes B (2004) A new method for measuring deformation on volcanoes and other natural terrains using InSAR persistent scatterers. *Geophys Res Lett* 31:L23611. doi:10.1029/2004GL021737
- Hooper A, Segall P, Zebker H (2007) Persistent scatterer InSAR for crustal deformation analysis, with application to Volcán Alcedo, Galápagos. *J Geophys Res* 112:B07407. doi:10.1029/2006JB004763
- Hooper A, Bekaert DPS, Spaans K, Arikan M (2012) Recent advances in SAR interferometry time series analysis for measuring crustal deformation. *Tectonophysics* 514–517:1–13. doi:10.1016/j.tecto.2011.10.013
- Hooper A, Bekaerti D, Spaans K (2013) StaMPS/MTI manual. Version 3.3b1. School of Earth and Environment, University of Leeds, UK
- Hu RL, Yue ZQ, Wang LC, Wang SJ (2004) Review on current status and challenging issues of land subsidence in China. *Eng Geol* 76:65–77
- IGME (1988) Memoria y mapa geológico de España, escala 1:50.000. Hoja de Montellano (1035)
- Jamiolkowski M, Ladd CC, Germaine J, Lancellotta R (1985) New developments in field and lab testing of soils. *Proceedings 11th international conference on soil mechanics and foundations engineering*, vol 1. San Francisco, pp 57–154
- Jiang L, Lin H, Cheng S (2011) Monitoring and assessing reclamation settlement in coastal areas with advanced InSAR techniques: Macao city (China) case study. *Int J Remote Sens* 32:3565–3588. doi:10.1080/01431161003752448
- Kirker AJ, Platt JP (1998) Unidirectional slip vectors in the western Betic Cordillera: implications for the formation of the Gibraltar arc. *J Geol Soc* 155:193–207. doi:10.1144/gsjgs.155.1.0193
- Leake SA (1990) Interbed storage changes and compaction in models of regional groundwater flow. *Water Resour Res* 26(9):1939–1950
- Martín-Algarra A, Vera JA (2004) La Cordillera Bética y las Baleares en el contexto del Mediterráneo occidental. In: Vera JA (ed) *Geología de España*. Soc Geol de Esp, Madrid, pp 352–354
- Massonnet E, Feigl KL (1998) Radar interferometry and its application to changes in the Earth's surface. *Rev Geophys* 36:441–500
- Mitchell JK (1998) Introduction: hazards in changing cities. *Appl Geogr* 18(1):1–6
- Ortiz-Zamora D, Ortega-Guerrero A (2010) Evolution of long-term land subsidence near Mexico City: review, field investigations, and predictive simulations. *Water Resour Res* 46(1):W01513. doi:10.1029/2008WR007398
- Osmanoglu B, Dixon TH, Wdowski S, Cabral-Cano E, Jiang Y (2011) Mexico City subsidence observed with persistent scatterer InSAR. *Int J Appl Earth Obs Geoinform* 13(1):1–12. doi:10.1016/j.jag.2010.05.009

- Pedreira A, Marín-Lechado C, Martos-Rosillo S, Roldán FJ (2012) Curved fold-and thrust accretion during the extrusion of a synorogenic viscous allochthonous sheet: The Estepa Range (External Zones, Western Betic Cordillera, Spain). *Tectonics* 31: TC4024. doi:[10.1029/2012TC003130](https://doi.org/10.1029/2012TC003130)
- Perissin D, Wang T (2011) Time-series InSAR applications over urban areas in China. *IEEE J Sel Top Appl Earth Obs Remote Sens* 4(1):92–100. doi:[10.1109/JSTARS.2010.2046883](https://doi.org/10.1109/JSTARS.2010.2046883)
- Poland JF (1961) The coefficient of storage in a region of major subsidence caused by compaction of an aquifer system. US geological survey professional paper 424-B: 52–54
- Rodríguez Ortiz JM, Mulas J (2002) Subsistencia generalizada en la ciudad de Murcia (España). In: Carcedo JA, Cantos JO (eds) *Riesgos Naturales*. Editorial Ariel, Barcelona, pp 459–463
- Rosen PA, Hensley S, Joughin IR, Li FK, Madsen SN, Rodrigues E, Goldstein RM (2000) Synthetic aperture radar interferometry. *Proc IEEE* 88:333–385
- Scharroo R, Visser P (1998) Precise orbit determination and gravity field improvement for the ERS satellites. *J Geophys Res* 103:8113–8127. doi:[10.1029/97JC03179](https://doi.org/10.1029/97JC03179)
- Shi LX, Bao MF (1984) Case history no. 9.2—Shanghai, China. In Poland JF (ed) *Guidebook to studies of land subsidence due to groundwater withdrawal*, UNESCO, Paris. <http://www.rcamnl.wr.usgs.gov/rgws/Unesco/PDF-Chapters/Chapter9-2.pdf>. Accessed 21 Dec 2015
- Sousa J, Hanssen R, Bastos L, Ruiz A, Perski Z, Gil A (2007) Ground subsidence in the Granada City and surrounding area (Spain) using DInSAR monitoring. In: *AGU Meeting 2007*. S. Francisco, USA, 10–14 Dec 2007
- Sousa J, Ruiz A, Hanssen R, Bastos L, Gil A, Galindo-Zaldívar J, Sanz de Galdeano C (2010) PS-InSAR processing methodologies in the detection of field surface deformation—study of the Granada Basin (Central Betic Cordilleras, Southern Spain). *J Geodyn* 49:181–189. doi:[10.1016/j.jog.2009.12.002](https://doi.org/10.1016/j.jog.2009.12.002)
- Sousa J, Hooper A, Hanssen R, Bastos L, Ruiz A (2011) Persistent scatterer InSAR: a comparison of methodologies based on a model of temporal deformation vs. spatial correlation selection criteria. *Remote Sens Environ* 115(10):2652–2663
- Sridharan A, Abraham BM, Jose BT (1991) Improved method for estimation of preconsolidation pressure. *Geotechnique* 41(2):263–268
- Tomás R, Márquez Y, Lopez-Sanchez JM, Delgado J, Blanco P, Mallorqui JJ, Martínez M, Herrera G, Mulas J (2005) Mapping ground subsidence induced by aquifer overexploitation using advanced differential SAR interferometry: Vega Media of the Segura River (SE Spain) case study. *Remote Sens Environ* 98:269–283. doi:[10.1016/j.enggeo.2010.06.004](https://doi.org/10.1016/j.enggeo.2010.06.004)
- Tomás R, Herrera G, Lopez-Sanchez JM, Vicente F, Cuenca A, Mallorqui JJ (2010) Study of the land subsidence in Orihuela City (SE Spain) using PSI data: distribution, evolution and correlation with conditioning and triggering factors. *Eng Geol* 116:105–121
- Wang C, Zhang H, Shan X, Ma J, Liu Z, Cheng S, Lu G, Tang Y, Guo Z (2004) Applying SAR interferometry for ground deformation detection in China. *Photogramm Eng Remote Sens* 70(10):1157–1165
- Xue YQ, Zhang Y, Ye SJ, Wu JC, Li QF (2005) Land subsidence in China. *Environ Geol* 48:713–720